Ab Initio Physics Considerations in the Design of Wireless and Non-Invasive Neural Recording Systems Using Magnetoelectric Nanoparticles

Elric Zhang[1], Ping Liang[2], Yagmur Akin Yildirim[1], Shawnus Chen[1], Mostafa Abdel-Mottaleb[3], Max Shotbolt[1], Zeinab Ramezani[1], Jieyuan Tian[1], Victoria Andre[1], and Sakhrat Khizroev[1]

[1]Department of Electrical and Computer Engineering, University of Miami, Coral Gables, FL 33146 USA
[2]Cellular Nanomed, Irvine, CA 93606 USA
[3]Massachusetts Institute of Technology, Cambridge, MA 02139 USA

Magnetoelectric nanoparticles (MENPs) provide a way to wirelessly and non-invasively record local neural activity deep in the brain. When administered into the brain, MENPs serve as auxiliary 3-D sources, thus offering a solution to the fundamental problem of inverse mathematics that has stifled the advancement in the field of wireless neural recording from its inception. Due to the magnetoelectric effect, the MENPs' magnetization is modulated by electric fields due to local neural activity. In turn, this modulated magnetization can be detected via modern magnetometers such as optical pumped magnetometers (OPMs) and nitrogen-vacancy (NV) center devices, already impacting the state of magnetoencephalography (MEG). This basic physics study discusses an aspect that has not been explored to date. There is a strong dependence of the MENPs-based recording on the specific location of the nanoparticles with respect to the neuronal microstructure. This analysis shows that one of the key conditions to enable the MENPs-based recording with a sub-10^{-3} cm^3 spatial resolution in real time would be to ensure the nanoparticles are located specifically on the membrane, where the neural-firing-caused electric field reaches its maximum value. One potential implementation of this high-resolution recording concept would be to integrate MENPs with the recently emerged magnetic particle imaging (MPI).

Index Terms— **Brain–machine interface (BMI), magnetoelectric nanoparticles (MENPs), neural recording, wireless BMI.**

I. Introduction

DESPITE decades of research, no viable technology to wirelessly and non-invasively record neural activity deep in the brain with adequately high spatial resolution exists today. Arguably, one of the main reasons is the fact that electric fields cannot be wirelessly transmitted from neurons (to sensors located outside the brain) without facing signal decay from the conductive brain tissue as well as interference by the rest of the brain circuitry [1]. In contrast, magnetic fields of reasonable strength, less than 10 kOe, propagate through the brain tissue without losses and do not significantly interfere with the brain's electric circuitry [2], [3]. There has been significant progress in reading brain activity magnetically using magnetometers such as superconducting quantum interference devices (SQUIDs) and optical pumped magnetometers (OPMs), which are already used in magnetoencephalography (MEG), as well as the emerging nitrogen-vacancy (NV) center devices currently considered for future MEG applications [4], [5], [6], [7], [8]. These sensors can detect extremely small magnetic fields, on the order of 10^{-9} Oe, over the skull due to neural activity deep in the brain. In regard to the SQUID technology, to provide an adequate signal-to-noise ratio (SNR), it requires special conditions such as cryogenic temperatures and field-shielded environments [9]. Nevertheless, though promising, all these technologies are fundamentally limited in their imaging capabilities. Arguably, most importantly, they cannot be used to solve the inverse mathematics problem of finding point sources in the 3-D (brain) space from 2-D boundary conditions [10]. Hence, it is difficult to see how they can be used for high-resolution mapping of neural activity deep in the brain in real time.

One robust engineering approach to overcome this problem would be to artificially introduce 3-D magnetic field sources deep in the brain, which have specific magnetic responses to local electric fields due to neural activity. The theoretical considerations in this article aim to achieve exactly that using magnetoelectric nanoparticles (MENPs) [11], [12], [13], [14].

Unlike any other nanoparticles, MENPs display a relatively strong magnetoelectric (ME) effect. According to the converse ME effect, when exposed to a local electric field, the magnetization of these nanoparticles changes accordingly [15]. In a trivial linear approximation, the dependence can be described by the following equation, derived from the phenomenological Landau theory of multiferroics [16]:

$$\Delta M_i = \alpha_i E_i \tag{1}$$

where ΔM_i is the change of the ith component of the magnetization, α_i is the converse ME coefficient along the ith central orientation, assuming a diagonal tensor, and E_i is the ith component of the applied electric field. This magnetization change is detectable using the aforementioned magnetometers. Therefore, if the nanoparticles are locally or globally distributed throughout the brain, the electric field due to neural firing in their vicinity will cause their magnetization change. There are two types of MENPs: single-phase multiferroics and

Manuscript received 29 May 2023; revised 25 July 2023; accepted 27 July 2023. Date of publication 3 August 2023; date of current version 26 September 2023. Corresponding author: S. Khizroev (e-mail: skhizroev@miami.edu).
Digital Object Identifier 10.1109/TMAG.2023.3300791

composite nanostructures such as the core–shell nanoparticles belonging to the 0–3 system. To date, core–shell MENPs have demonstrated a substantially higher ME coefficient, on the order of 1 V/cm/Oe, compared to the multiferroics, with an ME coefficient of $\ll$0.1 V/cm/Oe [11]. The origin of the ME effect in the core–shell MENPs is due to the strain propagation through the lattice-matched surface interface between the magnetostrictive core and the piezoelectric shell. The temporal response of these core–shell nanoparticles, limited by intrinsic physical resonances such as the ferromagnetic resonance, the dielectric resonance, and the mechanical resonance, lies in the sub-ns range [17], [18], [19]. Therefore, if integrated with existing magnetic imaging techniques such as magnetic resonance imaging (MRI) or the recently emerged magnetic particle imaging (MPI), the electric firing in the brain could be mapped in real time [20], [21], [22], [23]. Indeed, this hypothesis was proposed in [24]. Furthermore, COMSOL-based finite-element method calculations by Bok et al. [25] show that MPI could be used to map neural activity via MENPs. Given the relatively high temporal resolution of MPI, when integrated with MENPs, this imaging technique could provide neural activity mapping deep in the brain in real time [23], [26]. However, no physical model has been proposed to understand the fundamental limitations of the spatial resolution provided by the MENPs-based method to map the neural activity. Furthermore, these studies did not consider the recording efficacy's dependence on the specific target sites for MENPs in the central or peripheral nervous system (CNS and PNS). With the above said, the purpose of this study is to fill in this gap by providing theoretical insight into the fundamental limit of the spatial resolution of the promising wireless neural recording approach.

II. Physics of Recording With MENPs

According to (1), the larger the electric field variation during neural activity, the larger the magnetic signal detected through MENPs. Therefore, it is important to ensure that the nanoparticles are localized in the largest electric field variation regions of the nervous system, whether it is CNS or PNS. It is commonly assumed that the averaged electric field variation due to neural activity deep in the brain is on the order of 1 V/cm, with a dynamic response in the frequency range of approximately up to 1 kHz [25]. However, this value is averaged over a relatively large brain volume encompassing many neurons, thus not considering the nanoscale configuration of the cellular microstructure of individual neurons (Fig. 1). In other words, this value reflects the electric field variation in response to collective effects in relatively large neural circuits. In turn, the response from such collective effects does not provide information about the response from relatively small neural circuits or sub-circuits, or even single neurons. Therefore, to create a high-resolution recording approach, it is crucial to use the nanoscale model which considers the configuration of a single neuron. Such a single-neuron model must include both dielectric and conducting domains, e.g., conducting intracellular and extracellular microscale spaces separated by a dielectric membrane of a sub-10 nm thickness (Fig. 2). In fact, local electric field profiles in these two domain types, conducting and dielectric, respectively, substantially differ from each other; obviously, electric fields are significantly

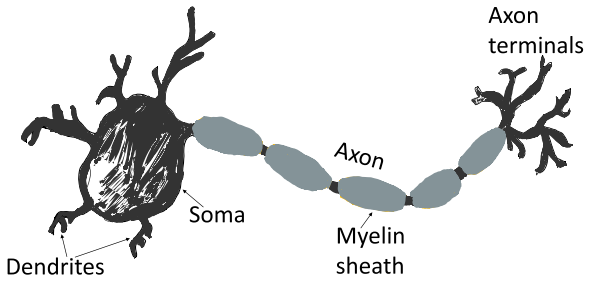

Fig. 1. Illustration (not to scale) of the basic neuron structure including: i) main body (soma); ii) dendrites and associated signal input terminals; and iii) axon and associated output terminals. After the charge energy delivered through dendrites reaches a threshold value, the neuron fires leading to a transient reversal of the charge in the soma (thus also reversing the electric field across the membrane), which in turn initiates an AP propagating along the axon to the axon terminals.

higher for the dielectric domain type. For example, given the membrane potential change (during a firing event) on the order of 10 mV and the membrane thickness on the order of 10 nm, the electric field change across the membrane during firing would be on the order of 100 000 V/cm. Obviously, only a fraction of this field would leak out in the immediate vicinity of the membrane due to the capacitive characteristic of the dielectric membrane and the conductive nature of the extracellular/intracellular space; free ions in the conductive space would relatively rapidly, with a characteristic time on the order of a millisecond, screen off any electric field leaking out from the membrane [27]. Therefore, if a nanoparticle is not in direct contact with the membrane, only a relatively small field, on the order of 1 V/cm, would be applied to the nanoparticle during a firing event. However, if a nanoparticle is in direct contact with the membrane, thus impeding a free flow of charged ions between the nanoparticle and the membrane, no full screening can take place. As a result, a significantly higher field, on the order of the field across the membrane, i.e., 100 000 V/cm, rather than the aforementioned averaged field on the order of 1 V/cm, would be applied to at least a portion of the nanoparticle, as described in the following in more detail. Assuming that the neuronal soma region contains the largest part of the neuronal membrane exposed to free ions in the extracellular/intracellular space, in this first order of approximation, it makes sense to consider nanoparticles in direct contact with the membrane surface of this particular region. In this case, the nanoparticles localized at the membrane surface experience a significant field variation during each neural firing event, i.e., when the electric field across the membrane reverses its sign. During this event, because of the ion-channel-controlled ion flows through the membrane, the net charges in the intracellular and extracellular spaces reverse their signs, initiating propagation of an action potential (AP) along the axon. During this intermediate event, lasting for approximately a millisecond, the membrane first depolarizes, thus leading to the electric field reversal across the membrane. Then, within a few milliseconds, it repolarizes back to the rest state, making the electric field across the membrane reverse back to its original orientation. The entire depolarization–repolarization event takes approximately 10 ms. Given the membrane thickness of 10 nm and the membrane potential in the rest and depolarized states of approximately -70 and $+50$ mV, respectively, the electric field

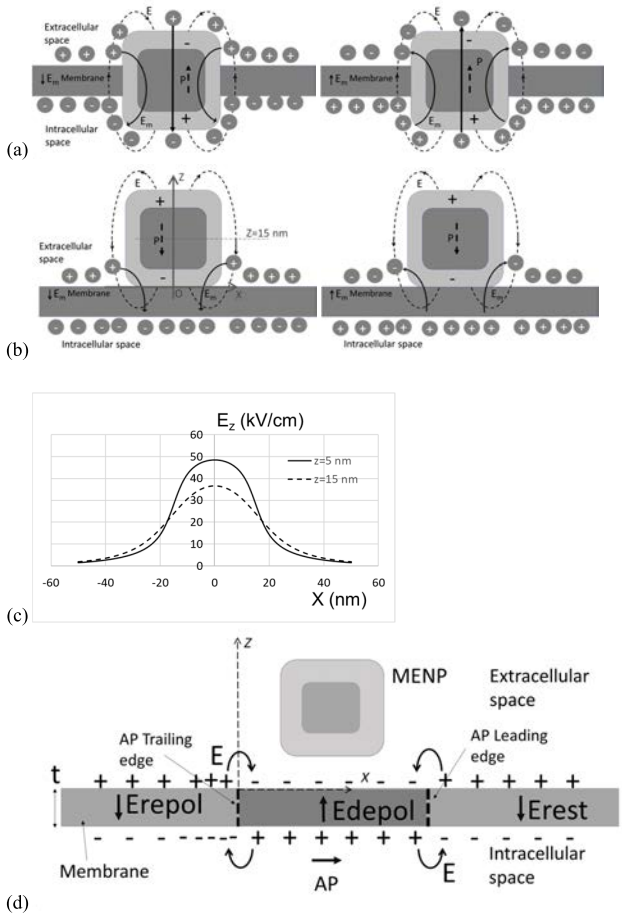

Fig. 2. Illustrations (not to scale) of the ion charge distributions in the intracellular and extracellular spaces during rest (left) and intermediate depolarized states of the membrane for two relative positions of MENPs with respect to the membrane: (a) nanoparticle symmetrically crosses the membrane and (b) nanoparticle is localized on the membrane surface. Positive and negative ions are shown by "plus" and "minus" circles, respectively. The electric fields due to the ion charge distribution and MENPs are shown by solid and broken arrows, respectively. E and P stand for the electric field and the nanoparticle's polarization, respectively. (c) z-component of the electric field versus the distance along the x-axis for the configuration shown in (b) left for $z = 5$ and 15 nm. (d) Illustration of charge distributions along a propagating AP when a MENP is not in direct contact with the membrane.

across the membrane in these two states would be approximately −70 000 and +50 000 V/cm, respectively. Again, these fields are significantly higher than the above averaged field on the order of 1 V/cm due to neural firing deep in the brain.

Hence, with respect to the strength of the electric field acting on MENPs, the nanoparticles could be divided into two major categories: i) MENPs in direct contact and ii) MENPs not in direct contact with the membrane.

The membrane is an essential entity to separate positive and negative free ions in the conductive extracellular and intracellular spaces. Bringing the dielectric MENPs into direct contact with the dielectric membrane effectively modifies the membrane geometry, thus affecting the charge distributions in the conductive intracellular and extracellular spaces. In this case, MENPs become effectively a part of the membrane, and they experience significantly larger field variations compared to the nanoparticles not in physical contact with the membrane. Arguably, from the symmetry perspective, there are two basic configurations for the nanoparticles in contact with the membrane, as illustrated in Fig. 2(a) and (b), respectively. If a nanoparticle can be localized across the membrane in the most symmetric configuration, free-moving ion charges will redistribute themselves around the nanoparticle's location to minimize the electrostatic energy, as shown in Fig. 2(a). The left and right parts of Fig. 2(a) illustrate ion charge distributions at rest and depolarized states, respectively. In a more realistic system, such a symmetric configuration might not be easy to achieve. Instead, a more likely scenario would be for the nanoparticle to have one of its sides interface with the membrane surface, e.g., using antibody targeting, as shown in Fig. 2(b). Even in this case, a significant fraction of the nanoparticle would be exposed to a field strong enough to have the magnetization saturated in both orientations, corresponding to the above rest and depolarized states, respectively. Coulomb's law can be used to evaluate the order of magnitude of the electric field inside the nanoparticle due to the electric fields generated by the ions around the membrane when the nanoparticle is in the configuration shown in Fig. 2(b). The evaluated perpendicular component of the electric field along horizontal lines parallel to the membrane surface 5 and 15 nm away from the nanoparticle' side touching the membrane is shown in Fig. 2(c). Here, it is assumed that the nanoparticle's shape is a cube with a 30 nm side, the membrane thickness is 10 nm, and the membrane is at rest. Obviously, the field will reverse its sign when the membrane is in the polarized state. In both field orientations, given the nanoparticle's size is comparable to the membrane thickness, a dominant portion of the nanoparticle volume is exposed to a relatively high electric field, with an amplitude ranging from 10^3 to 10^5 V/cm. In turn, given the ME coefficient, α, on the order of 1 G·cm/V, such high electric fields would be sufficient to fully saturate the nanoparticle's magnetization, assuming a characteristic saturation magnetization, M_S, of 1000 G, in both field orientations. Therefore, for both transitions, rest-to-depolarized state and depolarized-to-repolarized state, the magnetization change would be on the order of the saturation magnetization value, i.e., 1000 G. In contrast, if a MENP is not in a direct contact, the electric field applied to the nanoparticle due to the charge distribution changes during a neural firing event, say during an AP propagation, would be negligibly small because free ions screen off the charge variations at the membrane surface [Fig. 2(c)]. Assuming this field is on the order of 1 V/cm, the magnetization change would be on the order of 1 G, i.e., three orders of magnitude smaller than that in the case of MENPs being in direct contact with the membrane. Obviously, the recorded signal would also be significantly smaller for the nanoparticles not in direct contact with the membrane. The recorded signal is typically proportional to M^X, where X varies between 1 and 2, depending on the exact recording technique used to detect magnetic fields from the nanoparticles [28].

Given such a big difference between the signals emanating from the nanoparticles in direct contact and those not in direct contact with the membrane, it is straightforward to estimate the theoretical limits of measurable signals in the two cases. Obviously, the spatial resolution of MENPs-based imaging with the first type of nanoparticles would be substantially higher. Below, we evaluate the smallest volume which could be resolved with MENPs in direct contact with the membrane.

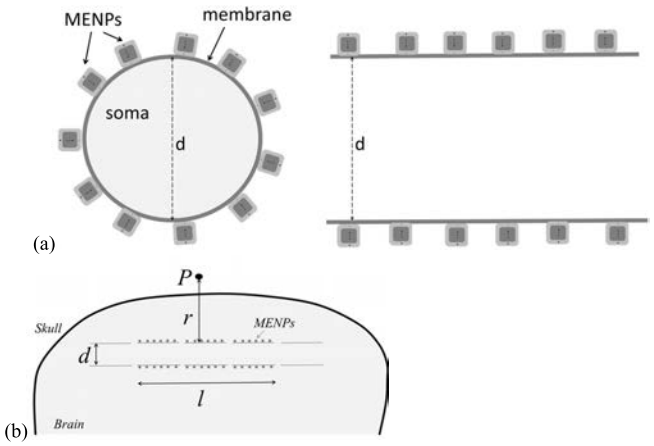

Fig. 3. (a) Illustration (not to scale) of a model of a spherically shaped neuronal soma with a diameter d and (right) a neuronal surface model made of two parallel surfaces separated by a distance d. (b) Illustration (not to scale) of the model showing the distribution of MENPs along two net membrane surfaces along a small area with a characteristic length l in a neural layer. The magnetic fields from the MENP dipoles on the two surfaces, determined by the neural state during a firing event, are oppositely directed. d is the distance between the surfaces (=neural diameter), and r is the distance between the neural layer and the point of observation. It is assumed that $d \ll r$ and $l \ll r$.

To simplify the description, it is assumed that the neuronal soma has a trivial spherical shape with a diameter d [Fig. 3(a)]. Assume nanoparticles are uniformly distributed over the soma membrane surface. As an example, neurons in the cerebral cortex can be considered. With a net thickness of about 2 mm, the cerebral cortex can be divided into six layers of interconnected neurons [29]. Then, in a trivial approximation, to evaluate the order of magnitude of the signal coming from MENPs localized in one of the layers, with respect to a measurement point, P, located outside the brain at a distance r away from the layer, the net membrane surface of all the neurons in the layer can be considered as two surfaces separated by d and on which the nanoparticles' dipole orientations are oppositely directed during a firing event, as shown in Fig. 3(b). It is assumed that the nanoparticles are localized within a relatively small area in the layer with a characteristic size l. Then, assuming $l \ll r$ and $d \ll r$, the net magnetic field due to the two oppositely directed contributions of the dipole magnetic fields would be on the order of

$$H \sim \frac{mN}{2}\left(\frac{1}{4\pi r^3} - \frac{1}{4\pi (r+d)^3}\right) \sim \frac{mNd}{r^4} \tag{2}$$

where m is the magnetic moment of one nanoparticle and N is the number of nanoparticles in the local region.

The average magnetic field above the skull due to neural activity in the whole human brain is known to be on the order of 10^{-9} Oe [5]. This value can be used as a reference field, an artificially chosen "noise" floor, to evaluate the effectiveness of the MENPs-based recording. As mentioned above, such a field value can be detected using the OPMs technology in a modern MEG system [4]. Assuming the saturation magnetization of 1000 G and the nanoparticle volume of 10^{-17} cc, the moment of one saturated nanoparticle, m, would be on the order of 10^{-14} erg/G. In other words, during each firing event, the nanoparticles on the membrane would change their magnetic moments by 10^{-14} erg/G. Then, according to (2), for $d = 0.01$ cm and $r = 1$ cm, approximately $N \sim 10^7$ nanoparticles would be required to generate a magnetic field to exceed the defined "noise" floor. In other words, only 10^7 MENPs located on the membrane can generate a magnetic field in magnitude comparable to that generated by the whole human brain. In previous studies, they placed over 10^{10} MENPs in the whole mouse brain to wirelessly modulate neural activity [30]. Assuming the nanoparticles are uniformly distributed over the brain and the average mouse brain is approximately 0.5 cm^3, 10^7 MENPs could resolve the neural activity from a region as small as 5×10^{-4} cm^3.

III. Discussion

The back-of-the-envelope physics calculations show that if MENPs, with currently available properties, could be placed directly on the membrane, they could wirelessly detect neural activity from a brain region as small as 5×10^{-4} cm^3. Placing nanoparticles on the membrane is vital to ensure the nanoparticles effectively become a part of the charge-separating dielectric membrane, thus being exposed to a relatively high electric field variation, on the order of 10^5 V/cm, during each neural firing event. In turn, assuming a linear ME effect, this would lead to the nanoparticle' magnetization change on the order of the saturation magnetization, thus ensuring the highest possible signal during each firing event. For comparison, the nanoparticles not in direct contact with the membrane would sense only a negligibly small fraction of this field, i.e., on average a field on the order of 1 V/cm, which is three orders of magnitude smaller than the field required to saturate the magnetization. As a result, the difference in the nanoparticle's magnetization variation due to firing, and consequently in the recorded signal, between these two cases is also three orders of magnitude. Therefore, our recommendation would be to functionalize the nanoparticles' surface with a bioreagent, e.g., an antibody, tailored to target the neuronal membrane, preferably the soma region, a neuron-targeting exosome [31], [32], [33], [34]. It can be noted that antibodies significantly vary in their size [35]. A smaller size and a more dielectric dependence of the antibody coating would be preferred to minimize the effective sacrificial spacing between the membrane and the nanoparticle. Another recently emerged promising approach is to coat nanoparticles with a membrane material to target the membrane [36].

To bring clarity into explaining the fundamental physics of the underlying mechanisms, this ab initio analysis makes certain oversimplified assumptions, e.g., assuming a linear ME effect throughout the entire field application range. In reality, the effect is non-linear in the entire range; therefore, the theoretical analysis could be significantly improved in the future. In addition, the analysis assumes that there are only two distinct regional domains for MENPs to be located with respect to the membrane, in direct contact and away, respectively. The nanoparticles in the former are subjected to a field on the order of 10^5 V/cm, which is approximately two orders of magnitude higher than the field required to saturate the magnetization, according to the above ideal linear ME dependence. In contrast, the nanoparticles in the latter are exposed to a significantly smaller field, on the order of 1 V/cm, which is three orders of magnitude smaller than the saturation field. Obviously, there is an intermediate location domain, where MENPs are not in direct contact with the

membrane, though remaining exposed to a field strong enough to be saturated (10^3–10^5 V/cm). This region is thus defined by an effective Debye length, which determines how quickly free ions in the intra- and extracellular spaces screen out the membrane's electric fields; this length is known to be less than a nanometer in neural circuits [37]. The current approximation does not consider this intermediate domain. Nevertheless, this analysis provides a helpful insight into the recording mechanism with MENPs. This insight helps easily distinguish the MENPs approach from competing approaches. For example, this analysis indicates that MENPs, if placed on the membrane, could be perfectly integrated with the current MEG technology to enable an unprecedent high spatial resolution for the emerging non-invasive recording approach. Furthermore, if integrated with MPI, such MENPs could enable high-resolution neural activity mapping in real time, thus answering many open questions related to the computing architecture of the brain as well as unlocking novel pathways to treat neurological diseases.

ACKNOWLEDGMENT

This work was supported in part by the Defense Advanced Research Projects Agency (DARPA) and Naval Information Warfare Center, Pacific (NIWC Pacific) under Contract N66001-19-C-4019; and in part by the National Science Foundation (NSF) under Award #ECCS-211082. Any opinions, findings and conclusions or recommendations expressed in this material are those of the author(s) and do not necessarily reflect the views of the DARPA or NIWC Pacific. Co-authors Sakhrat Khizroev and Ping Liang co-own a high-technology startup, Cellular Nanomed (CNMI), Irvine, CA, USA which aims to create the first high-resolution wireless non-invasive brain–machine interface (BMI).

REFERENCES

[1] Y. Huang et al., "Measurements and models of electric fields in the in vivo human brain during transcranial electric stimulation," *Brain Stimulation*, vol. 10, no. 4, pp. e25–e26, Jul. 2017.

[2] S. Singh, "Magnetoencephalography: Basic principles," *Ann. Indian Acad. Neurol.*, vol. 17, no. 5, p. 107, 2014.

[3] J. H. Duyn and J. Schenck, "Contributions to magnetic susceptibility of brain tissue," *NMR Biomed.*, vol. 30, no. 4, p. e3546, Apr. 2017.

[4] B. Wittevrongel et al., "Practical real-time MEG-based neural interfacing with optically pumped magnetometers," *BMC Biol.*, vol. 19, no. 1, pp. 1–12, Aug. 2021.

[5] R. Hari and R. Salmelin, "Magnetoencephalography: From SQUIDs to neuroscience neuroimage 20th anniversary special edition," *Neuroimage*, vol. 61, no. 2, pp. 386–396, 2012.

[6] R. Körber et al., "SQUIDs in biomagnetism: A roadmap towards improved healthcare," *Supercond. Sci. Technol.*, vol. 29, no. 11, Nov. 2016, Art. no. 113001.

[7] F. Cao et al., "OMMR: Co-registration toolbox of OPM-MEG and MRI," *Frontiers Neurosci.*, vol. 16, pp. 1–13, Sep. 2022.

[8] C. Schreyvogel, V. Polyakov, R. Wunderlich, J. Meijer, and C. E. Nebel, "Active charge state control of single NV centres in diamond by in-plane Al-Schottky junctions," *Sci. Rep.*, vol. 5, no. 1, Jul. 2015.

[9] H. M. Butler-Struben, S. M. Brophy, N. A. Johnson, and R. J. Crook, "In vivo recording of neural and behavioral correlates of anesthesia induction, reversal, and euthanasia in cephalopod molluscs," *Frontiers Physiol.*, vol. 9, Feb. 2018.

[10] R. Grech et al., "Review on solving the inverse problem in EEG source analysis," *J. Neuroeng. Rehabil.*, vol. 5, no. 1, pp. 1–33, 2008.

[11] P. Wang et al., "Colossal magnetoelectric effect in core-shell magnetoelectric nanoparticles," *Nano Lett.*, vol. 20, no. 8, pp. 5765–5772, 2020.

[12] N. A. Spaldin and M. Fiebig, "The renaissance of magnetoelectric multiferroics," *Science*, vol. 309, no. 5733, pp. 391–392, Jul. 2005.

[13] G. Srinivasan, "Magnetoelectric composites," *Ann. Rev. Mater. Res.*, vol. 40, pp. 153–178, Aug. 2010.

[14] V. Corral-Flores, D. Bueno-Baqués, and R. F. Ziolo, "Synthesis and characterization of novel $CoFe_2O_4$–$BaTiO_3$ multiferroic core–shell-type nanostructures," *Acta Mater.*, vol. 58, no. 3, pp. 764–769, Feb. 2010.

[15] S. Khizroev and P. Liang, "Engineering future medicines with magnetoelectric nanoparticles: Wirelessly controlled, targeted therapies," *IEEE Nanotechnol. Mag.*, vol. 14, no. 1, pp. 23–29, Feb. 2020.

[16] N. Kemmer, "Collected paper of LD Landau," *Proc. Phys. Soc. London*, vol. 88, no. 559, p. 247, 1966.

[17] N. Noginova, F. Chen, T. Weaver, E. P. Giannelis, A. B. Bourlinos, and V. A. Atsarkin, "Magnetic resonance in nanoparticles: Between ferro- and paramagnetism," *J. Phys., Condens. Matter*, vol. 19, no. 24, Jun. 2007, Art. no. 246208.

[18] A. Cafarelli et al., "Piezoelectric nanomaterials activated by ultrasound: The pathway from discovery to future clinical adoption," *ACS Nano*, vol. 15, no. 7, pp. 11066–11086, Jul. 2021.

[19] S. O'Brien, L. Brus, and C. B. Murray, "Synthesis of monodisperse nanoparticles of barium titanate: Toward a generalized strategy of oxide nanoparticle synthesis," *J. Amer. Chem. Soc.*, vol. 123, no. 48, pp. 12085–12086, Dec. 2001.

[20] E. E. Mason et al., "Concept for using magnetic particle imaging for intraoperative margin analysis in breast-conserving surgery," *Sci. Rep.*, vol. 11, no. 1, p. 13456, Jun. 2021.

[21] E. Mattingly, "A sensitive, stable, continuously rotating FFL MPI system for functional imaging of the rat brain," *Int. J. Magn. Part. Imag.*, vol. 8, no. 2, p. 13, 2022.

[22] Q. Chen and D. Levine, "Fast fetal magnetic resonance imaging techniques," *Topics Magn. Reson. Imag.*, vol. 12, no. 1, pp. 67–79, Feb. 2001.

[23] L. C. Wu et al., "A review of magnetic particle imaging and perspectives on neuroimaging," *Amer. J. Neuroradiol.*, vol. 40, no. 2, pp. 206–212, Feb. 2019.

[24] R. Guduru, P. Liang, M. Yousef, J. Horstmyer, and S. Khizroev, "Mapping the brain's electric fields with magnetoelectric nanoparticles," *Bioelectron. Med.*, vol. 4, no. 1, pp. 1–10, Dec. 2018.

[25] I. Bok, I. Haber, X. Qu, and A. Hai, "In silico assessment of electrophysiological neuronal recordings mediated by magnetoelectric nanoparticles," *Sci. Rep.*, vol. 12, no. 1, May 2022.

[26] A. Mohtashamdolatshahi et al., "In vivo magnetic particle imaging: Angiography of inferior vena cava and aorta in rats using newly developed multicore particles," *Sci. Rep.*, vol. 10, no. 1, Oct. 2020.

[27] J. V. Raimondo, R. J. Burman, A. A. Katz, and C. J. Akerman, "Ion dynamics during seizures," *Frontiers Cellular Neurosci.*, vol. 9, Oct. 2015.

[28] E. U. Saritas et al., "Magnetic particle imaging (MPI) for NMR and MRI researchers," *J. Magn. Reson.*, vol. 229, pp. 26–116, Apr. 2013.

[29] F. Briggs, "Organizing principles of cortical layer 6," *Frontiers Neural Circuits*, vol. 4, p. 3, Jan. 2010.

[30] T. Nguyen et al., "In vivo wireless brain stimulation via non-invasive and targeted delivery of magnetoelectric nanoparticles," *Neurotherapeutics*, vol. 18, no. 3, pp. 2091–2106, Jul. 2021.

[31] M. Mahn et al., "High-efficiency optogenetic silencing with soma-targeted anion-conducting channelrhodopsins," *Nature Commun.*, vol. 9, no. 1, p. 4125, Oct. 2018.

[32] G. Z. Jin et al., "Targeting with nanoparticles for the therapeutic treatment of brain diseases," *J. Tissue Eng.*, vol. 11, Jan. 2020, Art. no. 2041731419897460.

[33] M. Khongkow, T. Yata, S. Boonrungsiman, U. R. Ruktanonchai, D. Graham, and K. Namdee, "Surface modification of gold nanoparticles with neuron-targeted exosome for enhanced blood–brain barrier penetration," *Sci. Rep.*, vol. 9, no. 1, p. 8278, Jun. 2019.

[34] K. L. S. Cleary, H. T. C. Chan, S. James, M. J. Glennie, and M. S. Cragg, "Antibody distance from the cell membrane regulates antibody effector mechanisms," *J. Immunol.*, vol. 198, no. 10, pp. 3999–4011, May 2017.

[35] M. L. Chiu, D. R. Goulet, A. Teplyakov, and G. L. Gilliland, "Antibody structure and function: The basis for engineering therapeutics," *Antibodies*, vol. 8, no. 4, p. 55, Dec. 2019.

[36] Y. Han et al., "Macrophage membrane-coated nanocarriers co-modified by RVG29 and TPP improve brain neuronal mitochondria-targeting and therapeutic efficacy in Alzheimer's disease mice," *Bioactive Mater.*, vol. 6, no. 2, pp. 529–542, Feb. 2021.

[37] D. S. Peterka, H. Takahashi, and R. Yuste, "Imaging voltage in neurons," *Neuron*, vol. 69, no. 1, pp. 9–21, Jan. 2011.